metals

MDPI

Article

Effect of Plasma Nitriding and Oxidation on the Corrosion Resistance of 304 Stainless Steel in LiBr/H_2O and $CaCl_2$-LiBr-$LiNO_3$-H_2O Mixtures

A. K. Larios-Galvez [1,*], E. Vazquez-Velez [1], H. Martinez-Valencia [1] and J. G. Gonzalez-Rodriguez [2]

[1] Instituto de Ciencias Físicas, Universidad Nacional Autónoma de México, Av. Universidad, Cuernavaca 62209, Morelos, Mexico; velez.edna@icf.unam.mx (E.V.-V.); hm@icf.unam.mx (H.M.-V.)
[2] Center for Research in Engineering and Applied Sciences (CIICAP), Universidad Autónoma del Estado de Morelos, Av. Universidad 1001, Cuernavaca 62209, Morelos, Mexico; ggonzalez@uaem.mx
* Correspondence: agalvez@icf.unam.mx

Abstract: The effect of plasma nitriding and oxidation on the corrosion resistance of AISI 304 type stainless steel in LiBr/H_2O and $CaCl_2$-LiBr-$LiNO_3$-H_2O mixtures at 80 °C has been evaluated by using potentiodynamic polarization curves and electrochemical impedance spectroscopy techniques (EIS). Steel was plasma treated at 500 °C during 8 h under different atmospheres, nominally 20% N_2 + 80% H_2, 100% N_2 and 100% O_2. X-ray diffraction analysis (XRD) showed the presence of a CrN layer in nitrided specimens, whereas scanning electronic microscopy analysis revealed that specimen treated in the 20% N_2 + 80% H_2 atmosphere showed the thickest nitride layer. Specimens nitrided in the 20% N_2 + 80% H_2 atmosphere had the noblest open circuit potential value in both solutions, whereas potentiodynamic polarization curves indicated the formation of a passive layer. These specimens exhibited the lowest corrosion and passivation current density values. Corrosion process was under charge transfer control in both solutions regardless of the plasma treatment. The type of corrosion suffered by the steel under all treatments was the pitting type of corrosion. Pits density was the lowest for nitrides steels rather than that for untreated or pre-oxidized ones.

Keywords: plasma nitriding; pre-oxidation; stainless steel; LiBr; corrosion

check for updates

Citation: Larios-Galvez, A.K.; Vazquez-Velez, E.; Martinez-Valencia, H.; Gonzalez-Rodriguez, J.G. Effect of Plasma Nitriding and Oxidation on the Corrosion Resistance of 304 Stainless Steel in LiBr/H_2O and $CaCl_2$-LiBr-$LiNO_3$-H_2O Mixtures. *Metals* **2023**, *13*, 920. https://doi.org/10.3390/met13050920

Academic Editor: Mosab Kaseem

Received: 17 April 2023
Revised: 6 May 2023
Accepted: 7 May 2023
Published: 9 May 2023

Copyright: © 2023 by the authors. Licensee MDPI, Basel, Switzerland. This article is an open access article distributed under the terms and conditions of the Creative Commons Attribution (CC BY) license (https://creativecommons.org/licenses/by/4.0/).

1. Introduction

During the mid-1970s, Mario Molina and Frank Sherwood Rowland found that chlorofluorocarbons (CFC), chemical compounds made of carbon, fluor and chlorine are destroying the earth's stratosphere ozone layer [1]. CFC had been used as refrigerants and aerosol sprayers because they were neither toxic nor flammable; however, when they go up into the stratosphere, they are degraded by UV radiation, producing chlorine atoms. It has been estimated that a single chlorine atom can destroy 100,000 molecules of ozone. The destruction of the ozone layer causes damage to the marine ecosystems, skin cancer and some other eyes deceases [2]. As result of this, the Montreal Protocol suggested the reduction in the use of CFC and to replace them with less harmful refrigerants [3].

In the last decades, a large amount of refrigerants have been produced such as hydrocarbons, but they were rapidly discontinued due to their high flammability. Additionally, carbon dioxide was discontinued due to its low performance, and methylene and ethylene chloride were discontinued due to their high toxicity, among others [4,5]. Nevertheless, vapor compression refrigeration systems are widely used even though they use refrigerants that destroy the ozone layer, whereas absorption refrigerant systems use working fluids which do not cause damage to the environment [6,7].

Most widely used working fluids (absorber/refrigerant) in the absorption refrigerant systems include H_2O/NH_3 and LiBr/H_2O. Both solutions have low global heating potential, zero potential of ozone destruction and excellent thermodynamic properties;

however, NH_3 toxicity limits its use [8,9]. Despite the advantages offered by the LiBr/H_2O system, it has crystallization problems and causes severe corrosion problems to the metallic components [10–12]. Thus, several researchers have been investigating different working fluids with good thermal stability, without crystallization problems and that are less corrosive. Their results have shown that quaternary mixtures such as $CaCl_2$-LiBr-$LiNO_3$/H_2O [13] and $CaCl_2$-$LiNO_3$-KNO_3/H_2O [14] improved thermal properties and the crystallization temperature was 4% higher than that for the LiBr/H_2O mixture. However, the corrosion rate was increased for 1018 carbon and 316L type stainless steels, whereas that for copper and its alloys decreased. Thus, the search for new working fluids with good thermal properties and that are less corrosive continues.

Plasma nitriding is a thermochemical treatment that improves the surface properties of both ferrous and non-ferrous alloys [15]. This process consists in the incorporation of nitrogen atoms on the metal surface by a luminescent discharge at low pressure, which enhances the diffusion of atoms through interstitials sites of the metal crystalline structure, forming a nitride layer that can improve surface properties such as hardness, wear and corrosion resistance [16,17]. Some researchers have used plasma nitriding to improve the corrosion resistance of 316L, 430F and 304 type stainless steels [18–20], as well as 2205 type duplex stainless steel in acidic solutions. All of them reported the formation of CrN and FeN nitride layers on top of tested steels. In addition to this, some other researchers reported the improvement of the passive layer of 304 and 316L type stainless steels when they were plasma pre-oxidizing process [21–23]. Thus, the goal of this research work is to evaluate the effect of plasma nitriding and pre-oxidation treatments on the corrosion resistance of 304 type stainless steel in LiBr/H_2O and $CaCl_2$-LiBr-$LiNO_3$-H_2O solutions by using electrochemical techniques.

2. Experimental

2.1. Testing Material

Material used in this research work includes an AISI 304 type stainless steel with a chemical composition as given in Table 1. The steel came in a cylindrical bar with diameter of 0.95 cm, and specimens were cut in samples 1.0 cm long. They were grinded with SIC emery paper and polished with 1.0 mm Al_2O_3 powder, washed with water and, finally, ultrasonically cleaned in acetone.

Table 1. Chemical composition of tested 304 type stainless steel (wt. %).

Fe	C	Mn	P	S	Si	Cr	Ni
71.00	0.08	2.00	0.04	0.03	0.75	18.10	8.00

2.2. Plasma Nitriding and Pre-Oxidation Treatment

Plasma nitriding and pre-oxidation processes were carried out in a discharge chamber with two 5.0 cm diameter electrodes connected to a vacuum pump as schematically shown in Figure 1. Three different gas mixtures were employed including 20% N_2 + 80% H_2, 100% N_2 and 100% O_2. To produce the plasma, a voltage of 235 V was applied generating a current of 0.18 mA at a pressure of 2.0 torr and a temperature of 500 °C during 8 h.

2.3. Electrochemical Measurements

Potentiodynamic polarization curves and electrochemical impedance spectroscopy were the employed electrochemical tests. For this purpose, a conventional 200 mL three electrodes glass cell was used. During tests, Ag/AgCl and a 6.0 mm diameter graphite rode were used as a reference and counter electrode, respectively. The working electrode consisted of the 304 type stainless steel with an exposure working area of 0.71 cm^2. Testing solution included 55 (wt.%) LiBr/H_2O [12] and $CaCl_2$-LiBr-$LiNO_3$ (8.72:1:1)/H_2O [13] at 80 °C, which are the concentrations used under real working conditions. Before starting the tests, the open circuit potential value (OCP) was monitored during 60 min. EIS experiments were performed

at the free corrosion potential, E_{corr}, by applying a sinusoidal signal with an amplitude of ±10 mV peak-to-peak in frequency intervals of 0.01–100,000 Hz. Potentiodynamic polarization curves were carried out by polarizing the steel −700 mV more cathodic than the E_{corr} value, scanned towards the anodic direction at a scan rate of 1 mV/s finishing at a potential 400 mV more anodic than E_{corr}. For all tests, a 1000A Gamry Interface was used.

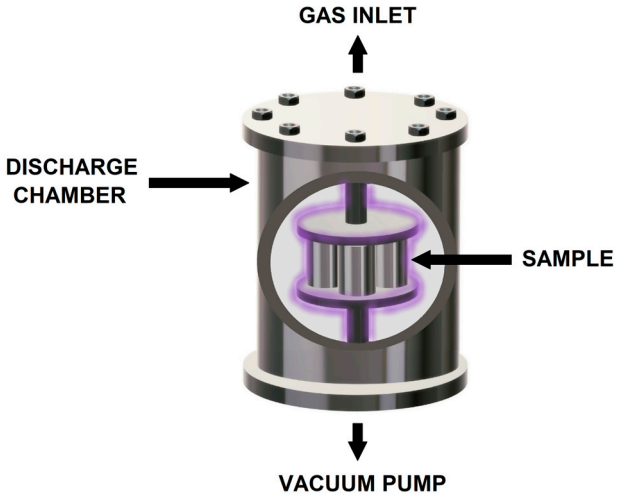


Figure 1. Scheme showing the plasma nitriding and pre-oxidation process.

2.4. Microstructural Characterization

In order to know the presence of any formed nitride or oxide by the plasma treatment, X-ray diffraction patterns (XRD) were performed with the use of a Rigaku DMAX 2200 equipment by using a CuKa (λ = 1.5418 Å) radiation with a scan rate of 1°/min. Morphology of the plasma-treated specimens before and after the corrosion tests was carried out with the aid of a Hitachi SU1510 scanning electronic microscope (SEM).

3. Results

3.1. X-ray Diffraction (XRD) Analysis

X-ray diffraction patterns of plasma-nitrided and pre-oxidized 304 type stainless steel under the different atmospheres are displayed in Figure 2. It can be seen from this figure that the phase corresponding to the steel, i.e., γ-Fe, is present in all cases at 2θ values of 44.3 degrees. The presence of the phase corresponding to chromium nitride, CrN, is present for steel nitrided in the 20% N_2 + 80% H_2 and pure N_2 atmospheres at 2θ values of 43.71° and 43.62°, respectively (ICDD PDF#11-0065). However, for the pre-oxidized specimen, it was not possible to detect any oxide layer on top of the steel, perhaps because it was very thin, and this might affect the corrosion resistance of the steel.

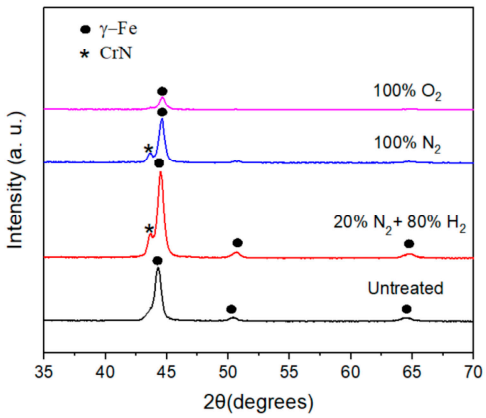


Figure 2. X-ray patterns obtained for 304 type stainless steel under different plasma treatments.

3.2. SEM Characterization

SEM micrographs of cross section corresponding to nitrided and pre-oxidized specimens in the different atmospheres are shown in Figure 3. The specimen nitrided in the 20% N_2 + 80% H_2 atmosphere exhibited a CrN layer thickness of 5.85 µm, whereas that formed on top of steel nitrided in pure N_2 has a thickness of 3.37 µm. A thicker film provides a better corrosion resistance to the surrounding environment because it will create a longer diffusion barrier and restrict corrosive ions from interacting with the metal causing its degradation. A thin layer of what seems to be Cr_2O_3 with a thickness less than 2.0 µm was observed for the pre-oxidized specimen. According to different authors, the use of H_2 improves the diffusion of the nitrogen atom to diffuse into the crystalline network of the steel [24,25]. Moskalioviene and Galdikas [26] showed that the addition of H_2 to the N_2 discharge in a concentration interval of 30 and 40% improves the penetration of nitrogen in 304 type stainless steel. Dalke et al. [27] revealed an increase in the nitride layer thickness by adding 10, 25 or 50% H_2, but this thickness decreased when 100% N_2 was used.

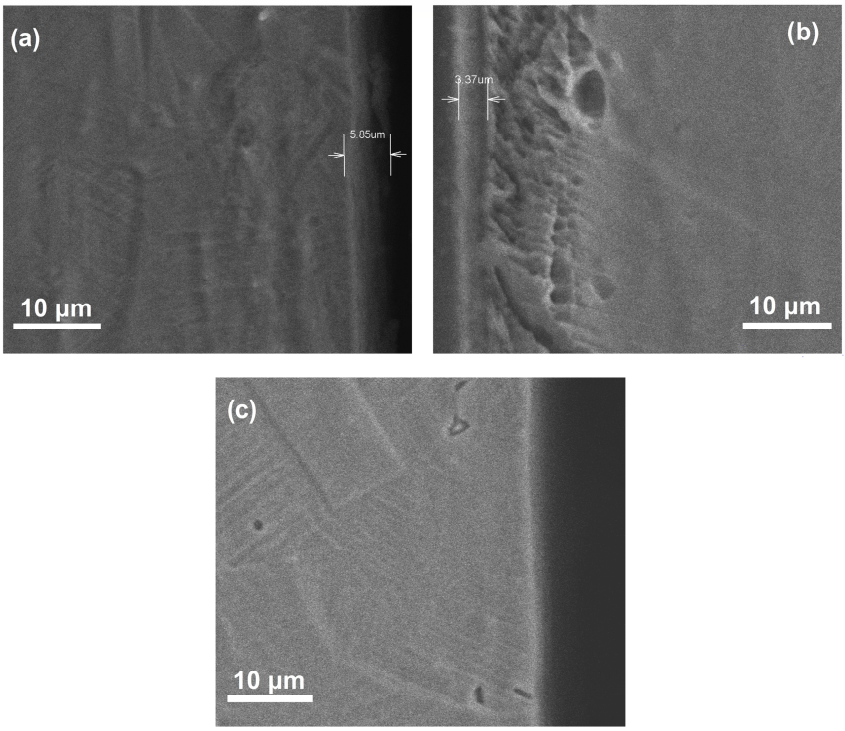


Figure 3. SEM cross section of 304 type stainless steel showing the steel (**a**) nitrided in 20% N_2 + 80% H_2, (**b**) nitride in 100% N_2 and (**c**) pre-oxidized in 100% O_2.

Energy dispersive X-ray analysis (EDS) is shown in Figure 4, it can observe the presence of elements such as Fe, Cr, O, Si, Mn and Ni for 304 type stainless steel sample at different atmospheres. The N element observed in the plasma-nitrided steel sample treated at 20% N_2 + 80% H_2 (Figure 4b) atmosphere and pure N_2 (Figure 4c) confirmed the presence of the chromium nitride layer (CrN).

Table 2 shows EDS quantitative analysis of 304 stainless steel samples at different atmospheres, and the O percentage increased in pre-oxidized steel by plasma from 3.45% to 23.00% (wt.), which indicates that the oxide layer formed on the surface of the steel treated is higher than in the untreated steel. On the other hand, the percentage of N in the sample treated with pure N_2 is slightly higher than the nitrided steel sample treated at 20% N_2 + 80% H_2 atmosphere. However, the O percentage is higher in the plasma-nitrided steel sample treated with pure N_2, which is more susceptible to corrosion.

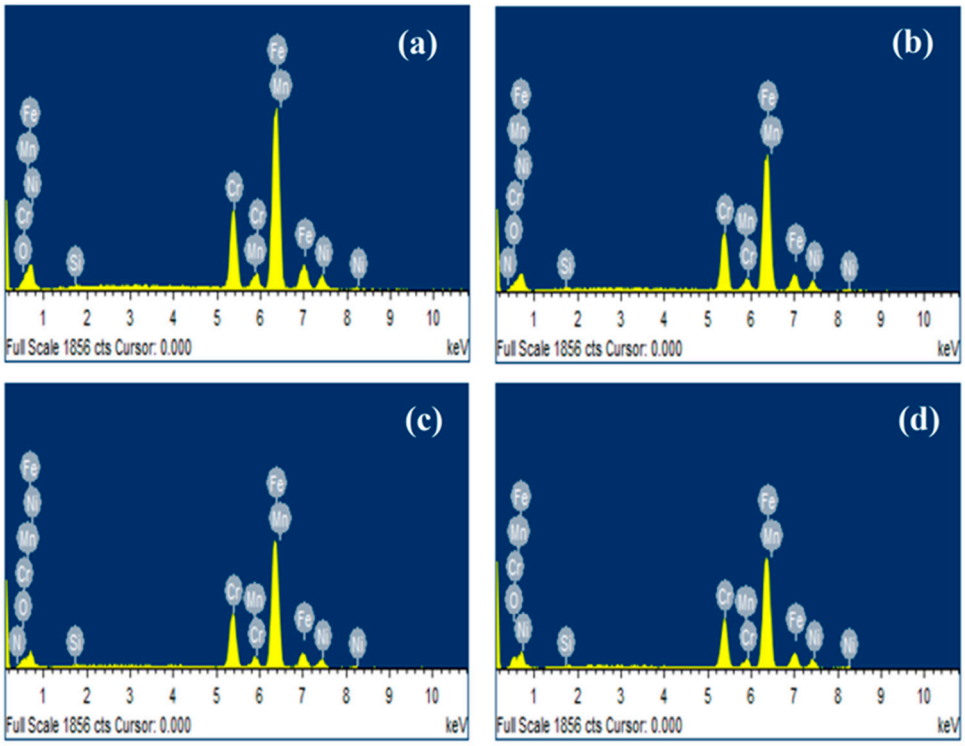


Figure 4. EDS analysis obtained for 304 type stainless steel (**a**) untreated, (**b**) nitrided in 20% N_2 + 80% H_2, (**c**) nitrided in 100% N_2 and (**d**) pre-oxidized in 100% O_2.

Table 2. EDS quantification analysis for 304 type stainless steel under different atmospheres.

Element	Weight %	Atomic %	Weight %	Atomic %	Weight %	Atomic %	Weight %	Atomic %
	Untreated		Nitrided in 20% N_2 + 80% H_2		Nitrided in 100% N_2		Pre-Oxidized in 100% O_2	
Fe K	64.16	57.86	48.72	27.91	41.10	20.05	51.54	32.31
Cr K	20.18	19.54	16.00	9.84	13.18	6.91	16.45	11.08
N K	-	-	13.84	31.62	15.54	30.22	-	-
O K	3.45	10.85	12.54	25.07	22.84	38.89	23.00	50.33
Si K	1.07	1.91	1.01	1.15	0.87	0.85	1.22	1.52
Mn K	4.50	4.13	3.01	1.75	2.70	1.34	51.54	32.31
Ni K	6.65	5.70	4.88	2.66	3.76	1.75	4.78	2.85

3.3. Electrochemical Tests

3.3.1. Open Circuit Potential

The variation in the OCP value for plasma-nitrided and pre-oxidized 304 type stainless steel in both LiBr/H_2O and $CaCl_2$-LiBr-$LiNO_3$/H_2O solutions at 80 °C are shown in Figure 5. In the LiBr/H_2O solution, Figure 5a, nitride 304 steel in the 20% N_2 + 80% H_2 atmosphere exhibited the noblest OCP value, close to −0.0 mV, followed by the pre-oxidized steel, which had a value around −100 mV, whereas the most active OCP value was exhibited by the steel nitride in 100% N_2. However, in all cases, the OCP value rapidly shifted into the active direction, especially the pre-oxidized specimen, indicating that the formation of any protective layer is being destroyed by the corrosive action of the LiBr/H_2O solution. The steel without plasma treatment, or untreated, had an OCP value which remained very constant as time elapsed, around −175 mV, very similar to the OCP value reached in the steady state condition by the steel nitrided in the 20% N_2 + 80% H_2 atmosphere. On the other hand, in the $CaCl_2$-LiBr-$LiNO_3$/H_2O solution, Figure 5b, the nobles OCP

value was exhibited for steel nitrided in the 20% N_2 + 80% H_2 atmosphere followed by the pre-oxidized steel, with values very similar to those shown in the LiBr/H_2O solution. The most active OCP value was for untreated steel, which exhibited a more active value than that in the LiBr/H_2O solution. One of the factors that leads to this situation is the presence of chloride and bromide ions in the $CaCl_2$-LiBr-$LiNO_3$/H_2O solution. On the other hand, $LiNO_3$ is a kind of anode inhibitor. Thus, in the LiBr/H_2O solution, we have only the effects of bromide ions, whereas in the $CaCl_2$-LiBr-$LiNO_3$/H_2O solution, we have two opposite effects: that for chloride and bromide ions and that for $LiNO_3$. Pre-oxidized steel exhibited an OCP value slightly nobler than that exhibited by untreated steel. Similar to the behaviour displayed in the LiBr/H_2O solution, the OCP values for nitrided steel in the 20% N_2 + 80% H_2 atmosphere as well as that for pre-oxidized specimen rapidly moved towards more noble values, indicating a lower susceptibility to be corroded, whereas the OCP value exhibited by the untreated steel shifted towards more active values, indicating the formation of a less protective layer of corrosion products. Towards the end of the test, the noblest OCP value was for steel nitrided in the 20% N_2 + 80% H_2 atmosphere, indicating the lowest susceptibility towards corrosion [28].

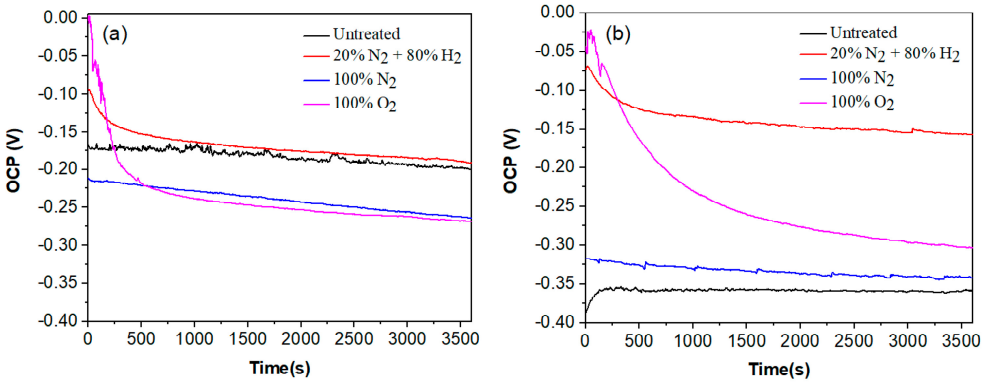


Figure 5. Variation in the OCP value with time for 304 type stainless steel under different plasma treatments and corroded in (**a**) LiBr/H_2O and (**b**) $CaCl_2$-LiBr-$LiNO_3$/H_2O solutions at 80 °C.

3.3.2. Potentiodynamic Polarization Curves

The effect of plasma nitriding or pre-oxidation on the polarization curves for 304 type stainless steel polarization curves in LiBr/H_2O and $CaCl_2$-LiBr-$LiNO_3$/H_2O solutions at 80 °C is shown in Figure 6, whereas electrochemical parameters such as E_{corr}, I_{corr}, pitting potential, E_{pit}, and passivation current density values, I_{pass}, are given in Table 3. It can be seen that regardless of the plasma treatment or testing solution, polarization curves displayed an active–passive behaviour, with the presence of a passive zone, very common in stainless steels due to the formation of a chromium oxide layer, Cr_2O_3, on top of the steel [29]. In LiBr/H_2O, Figure 6a, the noblest E_{corr} value was for the steel nitrided in the 20% N_2 + 80% H_2 atmosphere, with a value of −0.15 V, as compared to that for untreated steel, which has a value of −16 V. Steel treated either in pure N_2 or pre-oxidized exhibited more active E_{corr} values than the untreated steel. On the other hand, by nitriding the steel either in pure N_2 or in the 20% N_2 + 80% H_2 mixture, the I_{corr} value decreased slightly, whereas this value increased for the pre-oxidized steel. In a similar way, the pitting potential value was decreased with the plasma treatments since that value for untreated steel was of 0.12 V, whereas that for plasma-nitrided or pre-oxidized steel was between 0.01 and 0.08 V. However, the passivation current density value was the lowest for the plasma-treated steel than the untreated one.

On the other side, in the $CaCl_2$-LiBr-$LiNO_3$/H_2O solution, Figure 6b, the E_{corr} value became more positive for all the plasma treatments such as that evidenced by the OCP values obtained in this solution. The I_{corr} value was also decreased with the plasma treatments, obtaining the lowest value for the steel nitrided in the 20% N_2 + 80% H_2 mixture. The E_{pit} value became nobler for all plasma treatments, whereas the Ipas value decreased, obtaining

the lowest value for steel treated in the 20% N_2 + 80% H_2 mixture. Thus, the passive film properties such as the pitting potential and passivation current density value were improved with the plasma treatments in this solution due to the formation of the CrN layer, and likely as well as iron nitrides such as $Fe_{2-3}N$ and Fe_4N, especially for steel nitrided either in the 20% N_2 + 80% H_2 mixture, where the thickest CrN layer was obtained as explained above, or in pure N_2 [30–32]. However, for pre-oxidized specimens, electrochemical parameters such as I_{corr} and Ipas were improved, and these parameters were not as good as those obtained for nitrided specimens. It can be noticed that the values for both I_{corr} and I_{pas} were very similar in LiBr/H_2O and $CaCl_2$-LiBr-$LiNO_3$/H_2O solutions.

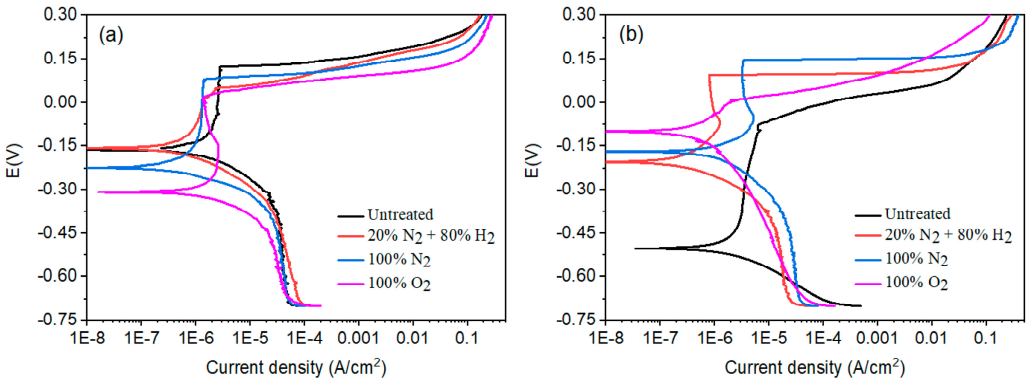


Figure 6. Effect of plasma treatment on the potentiodynamic polarization curves for 304 type stainless steel corroded in (**a**) LiBr/H_2O and (**b**) $CaCl_2$-LiBr-$LiNO_3$/H_2O solutions at 80 °C.

Table 3. Chemical electrochemical parameters obtained from potentiodynamic polarization curves.

Solution	Gas Concentration	E_{corr} (V)	I_{corr} (A/cm²)	E_{pit} (V)	I_{pas}
LiBr-H_2O	blank	−0.16	2.20×10^{-6}	0.12	2.82×10^{-6}
	20% N_2–80% H_2	−0.15	6.02×10^{-7}	0.05	1.37×10^{-6}
	100% N_2	−0.22	1.09×10^{-6}	0.08	1.09×10^{-6}
	100% O_2	−0.30	2.27×10^{-6}	0.01	1.41×10^{-6}
$CaCl_2$-LiBr-$LiNO_3$-H_2O	blank	−0.50	2.35×10^{-6}	−0.07	6.43×10^{-6}
	20% N_2–80% H_2	−0.20	4.12×10^{-7}	0.10	8.24×10^{-7}
	100% N_2	−0.17	1.06×10^{-6}	0.14	3.53×10^{-6}
	100% O_2	−0.09	3.52×10^{-7}	0.006	2.13×10^{-6}

3.3.3. Electrochemical Impedance Spectroscopy (EIS)

The effect of plasma nitriding and pre-oxidation on the EIS diagrams in the Nyquist and Bode formats for 304 type stainless steel immersed in LiBr/H_2O and $CaCl_2$-LiBr-$LiNO_3$/H_2O solutions at 80 °C are given in Figures 7 and 8, respectively. Nyquist diagrams, Figures 7a and 8a, indicate that data display a single capacitive, depressed semicircle with its centre at the real axis, indicating that the corrosion process is under charge transfer control and was not affected by the surface treatment given to the steel. In the LiBr/H_2O solution, Figure 7a, the biggest semicircle diameter correspond to the steel nitrided in 20% N_2 + 80% H_2, followed by the one nitrided in pure N_2, indicating that the formed nitride is protecting the steel against corrosion. On the other side, the lowest semicircle diameter corresponds to the plasma-pre-oxidized steel, indicating that the formed oxide did not protect the steel. Unlike this, in the $CaCl_2$-LiBr-$LiNO_3$/H_2O solution, Figure 8a, the biggest semicircle diameter was obtained for the steel nitrided in pure N_2, followed by the steel nitrided in 20% N_2 + 80% H_2, i.e., the highest corrosion resistance was obtained by nitrided steels. The smallest semicircle diameter was obtained by the untreated steel, indicating that both nitriding and pre-oxidation treatments improved the steel corrosion resistance. One possible explanation for this is that by pre-oxidizing the steel, the oxide

layer formed on the surface of the steel is thicker than the formed on the untreated steel, and the pre-oxidation treatment improve the steel corrosion resistance [33].

On the other hand, Bode diagrams in the modulus format, Figures 7b and 8b, indicate that in both solutions, and were obtained for the steel nitrided in 20% N_2 + 80% H_2 and N_2. This indicates that plasma nitriding efficiently improves the steel corrosion performance in both LiBr/H_2O (Figure 7b) and $CaCl_2$-LiBr-$LiNO_3$/H_2O solutions. Bode diagrams in the phase angle format show that this remains very constant over a wide interval of frequency, between 1 and over 1000 Hz, typical of the formation of a very protective passive layer, indicating the presence of two time constants. The first-time constant is associated with the electrochemical processes that occur at the metal/double electrochemical layer interface, whereas the second one corresponds to the electrochemical processes that occur at the steel/nitride or steel/oxide interface. The biggest phase angle in both solutions was obtained for the steel nitrided in pure N_2, with values higher than 75°, typical of a metal covered with a very protective layer formed on its surface [34]. In both solutions, the phase angle values were higher than 60°, which indicates the formation of very protective either nitrides or oxides.

EIS data for 304 type stainless steel exposed to LiBr/H_2O and $CaCl_2$-LiBr-$LiNO_3$/H_2O solutions at 80 °C can be simulated by using electric circuit shown in Figure 9. In this figure, R_{ct} represents the charge transfer resistance, and C_{dl} represents the double electrochemical layer capacitance which has been replaced by a phase constant element CPE_{dl} due to heterogeneities present on the steel surface and to the surface roughness, etc., which give rise to depressed semicircles as those shown in Figures 7a and 8a. The resistance of the oxide or nitrides present on top of the steel is represented by R_{ox}, which has been replaced by a constant phase element, CPE_{ox}, for the same reasons given above. The impedance of a constant phase element is expressed by the following:

$$Z_{CPE} = \frac{1}{Y_0(j\omega)^n} \quad (1)$$

where ω is the angular frequency, Y_0 a proportionality constant, and n represents the deviation of a pure capacitor and gives an idea of the surface roughness [35]. Parameters obtained from fitting EIS data with the use of circuit shown in Figure 9 are given on Tables 3 and 4 for tests in LiBr/H_2O and $CaCl_2$-LiBr-$LiNO_3$/H_2O solutions, respectively. In these tables, polarization resistance value, R_p, is the sum of R_{ct} and R_{ox}. It can be seen from these tables that the solution resistance, R_s, is more or less constant regardless of the steel plasma treatment, with values fluctuating between 1 and 3 ohm cm^2 due to the high solution conductivity. An interesting issue is that the nitride or oxide layer resistance value, R_{ox}, is significantly higher than that for the charge transfer resistance value, R_{ct}, which indicates that the steel corrosion resistance is given by the oxide or nitride formed on the steel. Thus, in LiBr/H_2O, the R_{ox} value was maximum for steel nitride in the 20% N_2 + 80% H_2 atmosphere followed by the treatment in pure N_2, whereas the lowest R_{ox} value was obtained in 100% O_2. Similarly, for the tests carried out in the $CaCl_2$-LiBr-$LiNO_3$/H_2O solution, the maximum R_{ox} value was, once again, for steel nitride in pure N_2 followed by the steel nitride in 20% N_2 + 80% H_2 and the pre-oxidized specimen. Conversely to this, in the LiBr solution, the CPE_{ox} value was lowest for steel nitride in the 20% N_2 + 80% H_2 atmosphere, whereas in the $CaCl_2$-LiBr-$LiNO_3$/H_2O solution, the CPE_{ox} value was lowest for the pre-oxidized steel in 100% O_2. In both corrosive solutions, the highest value was obtained for untreated steel. In addition to this, an n value close to 1.0 indicates a low surface roughness due to a low steel corrosion dissolution rate, whereas a value close to 0.5 indicates a high surface roughness due to a high steel corrosion rate. Tables 4 and 5 show that the highest n_{ox} and n_{dl} values were obtained for nitride steel, whereas untreated steel had one of the lowest n_{ox} and n_{dl} values. These results indicate that the corrosion resistance of 304 type stainless steel in LiBr/H_2O and $CaCl_2$-LiBr-$LiNO_3$/H_2O solutions are significantly improved by the plasma nitriding or oxidizing treatments as reported in the existing literature.

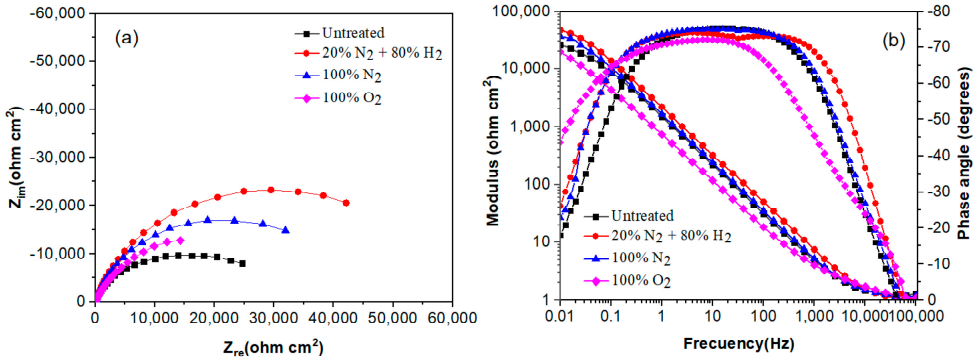


Figure 7. Effect of plasma treatment on the (**a**) Nyquist and (**b**) Bode plots for 304 type stainless steel corroded in $LiBr/H_2O$ at 80 °C.

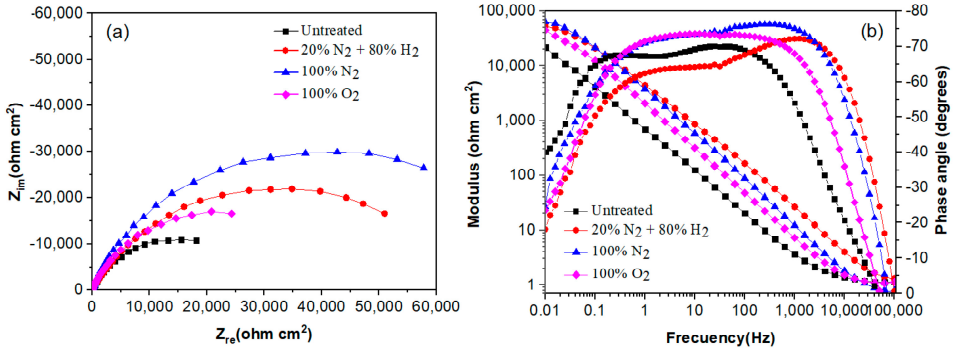


Figure 8. Effect of plasma treatment on the (**a**) Nyquist and (**b**) Bode plots for 304 type stainless steel corroded in $CaCl_2$-LiBr-$LiNO_3/H_2O$ at 80 °C.

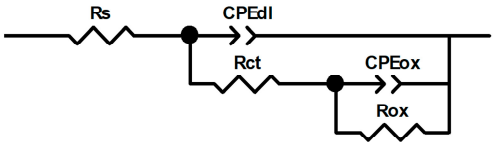


Figure 9. Electric circuit used to simulate the EIS data for 304 type stainless steel exposed to $LiBr/H_2O$ and $CaCl_2$-LiBr-$LiNO_3/H_2O$ at 80 °C.

Table 4. Electrochemical parameters obtained from the fit of EIS data for 304 corroded in $LiBr/H_2O$ at 80 °C.

Gas Atmosphere	R_s (ohm cm^2)	CPE_{ox} ($s^n S$)	n_{ox}	R_{ox} (ohm cm^2)	CPE_{dl} ($s^n S$)	n_{dl}	R_{dl} (ohm cm^2)	R_p (ohm cm^2)
None	1.2	2.4×10^{-4}	0.8	21,791	2.6×10^{-4}	0.8	6321	28,113
20% N_2 + 80% H_2	1.0	1.0×10^{-4}	0.9	53,782	2.1×10^{-3}	0.9	499	54,282
100% N_2	1.1	2.2×10^{-4}	0.9	30,782	2.1×10^{-4}	0.9	6499	37,282
100% O_2	1.3	8.5×10^{-4}	0.7	15,782	4.3×10^{-4}	0.7	6499	22,282

Table 5. Electrochemical parameters obtained from the fit of EIS data for corroded in $CaCl_2$-LiBr-$LiNO_3/H_2O$ at 80 °C.

Gas Atmosphere	R_s (ohm cm^2)	CPE_{ox} ($s^n S$)	n_{ox}	R_{ox} (ohm cm^2)	CPE_{dl} ($s^n S$)	n_{dl}	R_{dl} (ohm cm^2)	R_p (ohm cm^2)
None	1.48	4.3×10^{-4}	0.7	20,181	4.1×10^{-4}	0.7	3181	23,363
20% N_2 + 80% H_2	1.04	5.4×10^{-5}	0.8	59,176	5.3×10^{-5}	0.9	267	59,443
100% N_2	0.84	4.1×10^{-5}	0.9	62,429	2.1×10^{-5}	0.8	3314	65,744
100% O_2	2.38	3.6×10^{-5}	0.8	29,027	3.1×10^{-4}	0.8	5963	34,992

3.4. Surface Analysis

SEM micrographs of the surface of plasma treated 304 type stainless steel corroded in $LiBr/H_2O$ and $CaCl_2$-LiBr-$LiNO_3/H_2O$ at 80 °C are shown in Figures 10 and 11, respectively. These figures show that regardless of the steel condition, the presence of localized type of corrosion such as pits can be observed on the surface specimens due to the presence of both Cl^- and Br^- ions in the solutions. However, the surface damage, due to a lower density of pits, is less severe in $LiBr/H_2O$ than in $CaCl_2$-LiBr-$LiNO_3/H_2O$. It can be also shown that the untreated and pre-oxidized steel, Figure 10a,d and Figure 11a,d, exhibited the highest pits density, and, thus, a major surface damage, whereas specimens nitride either in 20% N_2 + 80% H_2 or pure N_2, Figure 10b,c and Figure 11b,c, exhibited the lowest pits density, and, thus, the surface damage was much less. This shows that nitride layer formed on top of 304 steel protects it against corrosion in $LiBr/H_2O$ and $CaCl_2$-LiBr-$LiNO_3/H_2O$ solutions, whereas by pre-oxidizing the steel was not as effective as nitriding to protect the steel from the aggressive action of these environments.

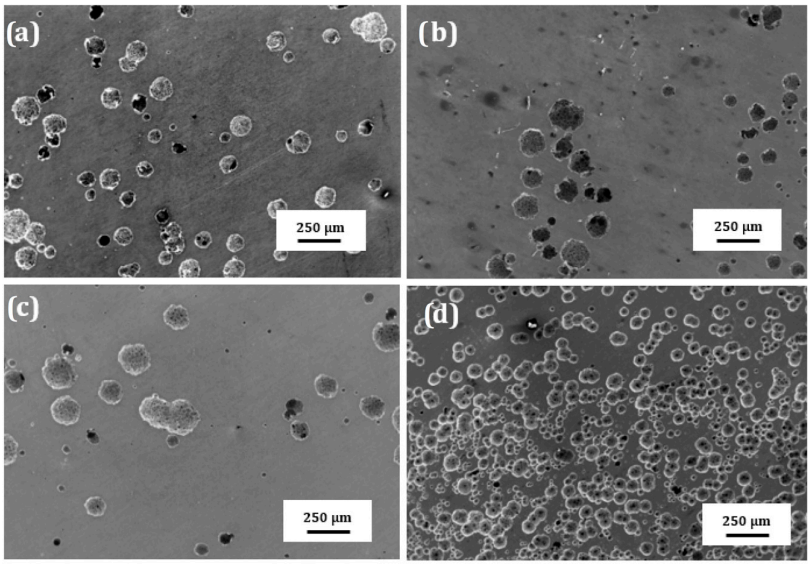


Figure 10. SEM micrographs of the surface of 304 steel in the (**a**) untreated condition and (**b**) nitrided in 20% N_2 + 80% H_2, (**c**) nitrided in 100% N_2 and (**d**) pre-oxidized in 100% O_2 corroded in $LiBr/H_2O$ at 80 °C.

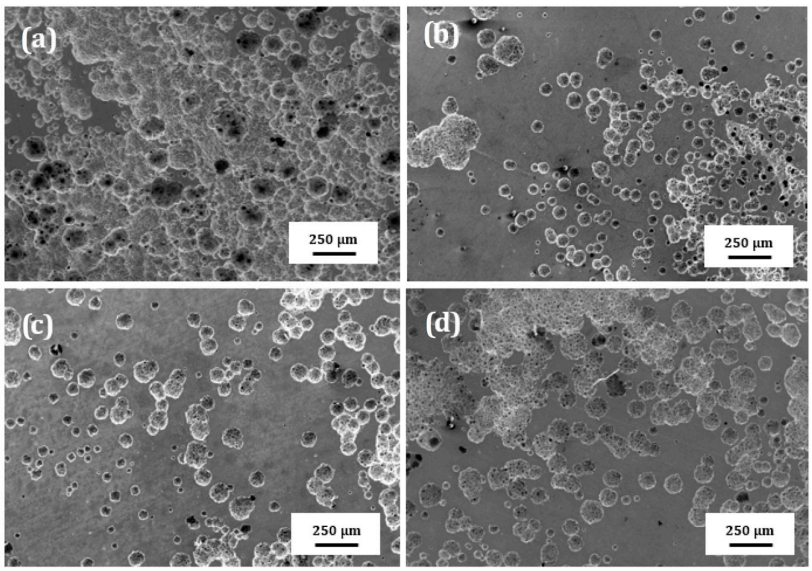


Figure 11. SEM micrographs of 304 steel in the (**a**) untreated condition and (**b**) nitrided in 20% N_2 + 80% H_2, (**c**) nitrided in 100% N_2 and (**d**) pre-oxidized in 100% O_2 corroded in $CaCl_2$-LiBr-$LiNO_3/H_2O$ at 80 °C.

4. Conclusions

- By plasma nitriding 304 type stainless steel either in 20% N_2 + 80% H_2 or pure N_2 at a pressure of 2.0 torr and a temperature of 500 °C for 8 h, a nitride layer 5.85 and 3.37 μm thick, respectively, is produced. This layer is composed mainly of γ-Fe and CrN.
- The noblest OCP value in both LiBr/H_2O and $CaCl_2$-LiBr-$LiNO_3$/H_2O solutions was for steel nitrided in the 20% N_2 + 80% H_2 atmosphere, whereas the most active value was for both untreated or pre-oxidized steel.
- Polarization curves showed the presence of a passive layer in all cases regardless of the surface steel condition in both solutions. The lowest Ipas was obtained for nitrided steels. In LiBr/H_2O, the E_{pit} value was only marginally affected by the plasma treatments, but in $CaCl_2$-LiBr-$LiNO_3$/H_2O the noblest values were obtained for nitrided steels. Similarly, the lowest corrosion current density value was obtained for steel nitrided in the 20% N_2 + 80% H_2 atmosphere.
- EIS results showed that the corrosion process is under charge transfer control regardless of the surface treatment in both LiBr/H_2O and $CaCl_2$-LiBr-$LiNO_3$/H_2O solutions. The film resistance of the nitride layers was higher than that for untreated or pre-oxidized steel, giving a higher corrosion resistance to the steel.
- The type of corrosion damage that the steel exhibited in both LiBr/H_2O and CaCl2-LiBr-$LiNO_3$/H_2O solutions was the pitting type of corrosion. However, the highest damage was for either untreated or pre-oxidized steel, whereas the lowest damage was for nitride steels.

Author Contributions: Conceptualization and methodology, A.K.L.-G.; software and validation, E.V.-V.; data acquisition and supervision, H.M.-V.; formal analysis and investigation, J.G.G.-R.; project administration and funding acquisition, H.M.-V. All authors have read and agreed to the published version of the manuscript.

Funding: This research received no external funding.

Data Availability Statement: Data are available upon request.

Acknowledgments: This research work was carried out at the Instituto de Ciencias Físicas of the Universidad Nacional Autónoma de México (UNAM), supported by the Dirección General de Asuntos del Personal Académico (DGAPA) through the Programa de Becas Posdoctorales-UNAM. Authors also would like to acknowledge the unvaluable help of J. Campos-Alvarez (IER-UNAM) for his help in the use of the SEM.

Conflicts of Interest: The authors declare no conflict of interest.

References

1. Bricker, B. Scientific Counterpublics: In Defense of the Environmental Scientist as Public Intellectual. *Topoi* **2019**, *38*, 681–692. [CrossRef]
2. Ali, S.R. Review on ozone depletion and global warming. *Int. Multidiscip. Res. J.* **2021**, *11*, 2072–2078.
3. Montzka, S.A.; Dutton, G.S.; Portmann, R.W.; Chipperfield, M.P.; Davis, S.; Feng, W.; Theodoridi, C. A decline in global CFC-11 emissions during 2018−2019. *Nature* **2021**, *590*, 428–432. [PubMed]
4. Mohammadi, K.; Powell, K. Thermodynamic and economic analysis of different cogeneration and trigeneration systems based on carbon dioxide vapor compression refrigeration systems. *Appl. Therm. Eng.* **2020**, *164*, 114503. [CrossRef]
5. Venkatarathnam, G.; Murthy, S.S. Refrigerants for Vapour Compression Refrigeration Systems. *Resonance* **2012**, *17*, 139–162. [CrossRef]
6. Sleiti, A.K.; Al-Ammari, W.A.; Al-Khawaja, M. Review of innovative approaches of thermo-mechanical refrigeration systems using low grade heat. *Int. J. Energy Res.* **2020**, *44*, 9808–9838. [CrossRef]
7. Chowdhury, S.; Roy, R.; Mandal, B.K. A Review on Energy and Exergy Analysis of Two-Stage Vapour Compression Refrigeration System. *Int. J. Air-Cond. Refrig.* **2019**, *27*, 9. [CrossRef]
8. Luberti, M.; Di Santis, C.; Santori, G. Ammonia/Ethanol Mixture for Adsorption Refrigeration. *Energies* **2020**, *13*, 983. [CrossRef]
9. Vuppaladadiyam, A.K.; Antunes, E.; Vuppaladadiyam, S.S.V.; Baig, Z.T.; Subiantoro, A.; Lei, G.; Leu, S.; Sarmah, A.K.; Duan, H. Progress in the development and use of refrigerants and unintended environmental consequences. *Sci. Total Environ.* **2022**, *823*, 153670. [CrossRef]

10. Zhang, X.; Qiu, Y.; Zhu, W.; Yu, W.; Cao, Y.; Wang, X.; Liang, Y. Corrosion behavior of 316 stainless steel, copper, and brazed joint in lithium bromide solution at different temperatures. *Mater. Test.* **2022**, *64*, 67–77. [CrossRef]
11. Elhamid, S.A.; Meleigy, A.E.; Attia, A.; Warraky, A.E.; Abd-El-Wahab, S. Corrosion Behaviour of Copper– nickel Alloys in LiBr Solutions: A Comparative Study. *Egypt. J. Chem.* **2020**, *63*, 907–919. [CrossRef]
12. Li, N.; Luo, C.; Su, Q. A Working pair of $CaCl_2$–LiBr–$LiNO_3$/H_2O and its application in a single-stage solar-driven absorption refrigeration cycle. *Int. J. Refrig.* **2018**, *86*, 1–13. [CrossRef]
13. Li, Y.; Li, N.; Luo, C.; Su, Q. Study on a Quaternary Working Pair of $CaCl_2$-$LiNO_3$-KNO_3/H_2O for an Absorption Refrigeration Cycle. *Entropy* **2019**, *21*, 546. [CrossRef] [PubMed]
14. Ravindra, K.; Bhardwaj, D.; Sharma, Y.C. A review on Plasma Ion Nitriding (PIN) process. i-manager's. *J. Mater. Sci.* **2018**, *6*, 31.
15. De Souza Lamim, T.; Salvaro, D.; Oss Giacomelli, R.; Binder, R.; Binder, C.; Klein, A.N.; Biasoli de Mello, J.D. Plasma nitrided compound layers in sintered parts: Microstructures and wear mechanisms. *Wear* **2021**, *477*, 203810. [CrossRef]
16. Jasinski, J.J.; Fraczek, T.; Kurpaska, L.; Lubas, M.; Sitarz, M. Investigation of nitrogen transport in active screen plasma nitriding processes e Uphill diffusion effect. *J. Mol. Struct.* **2018**, *484*, 710–715. [CrossRef]
17. Huang, Z.; Guo, Z.; Liu, L.; Guo, Y.; Chen, J.; Zhang, Z.; Li, J.; Li, Y.; Zhou, Y.; Liang, Y. Structure and corrosion behavior of ultra-thick nitrided layer produced by plasma nitriding of austenitic stainless steel. *Surf. Coat. Technol.* **2021**, *405*, 126689. [CrossRef]
18. Alphonsa, J.; Mukherjee, S.; Raja, V.S. Study of plasma nitriding and nitrocarburizing of AISI 430F stainless steel for high hardness and corrosion resistance. *Corros. Eng. Sci. Technol.* **2018**, *53*, 51–58. [CrossRef]
19. Shen, H.; Wang, L.; Sun, J. Characteristics and properties of Cr-N compound layer produced by plasma nitriding of Cr-electroplated of AISI 304 stainless steel. *Surf. Coat. Technol.* **2020**, *385*, 125450. [CrossRef]
20. Naeem, M.; Iqbal, J.; Zakaullah, M.; Shafiq, M.; Mujahid, Z.I.; Díaz-Guillén, J.C.; Lopez-Badillo, C.M.; Sousa, R.R.M.; Khana, M.A. Enhanced wear and corrosion resistance of AISI-304 steel by duplex cathodic cage plasma treatment. *Surf. Coat. Technol.* **2019**, *375*, 34–45. [CrossRef]
21. Núñez, Y.; Mafra, M.; Morales, R.E.; Borges, P.C.; Pintaude, G. The effect of plasma nitriding on the synergism between wear and corrosion of SAF 2205 duplex stainless steel. *Ind. Lubr. Tribol.* **2020**, *72*, 1117–1122. [CrossRef]
22. Ma, L.; Pascalidou, E.M.; Wiame, F.; Zanna, S.; Maurice, V.; Marcus, P. Passivation mechanisms and pre-oxidation effects on model surfaces of FeCrNi austenitic stainless steel. *Corros. Sci.* **2020**, *167*, 108483. [CrossRef]
23. Huang, X.; Li, X.; Zhan, Z.; Xiao, K.; Fang, X.; Li, Z. Effect of Long-Term Pre-oxidation on the Corrosion Rate of 316L Stainless Steel in a High-Temperature Water Environment. *J. Mater. Eng. Perform.* **2022**, *31*, 7935–7944. [CrossRef]
24. Naofumi, O.; Koyo, M.; Mitsuhiro, H.; Kenji, K. Investigation of admixed gas effect on plasma nitriding of AISI316L austenitic stainless steel. *Vacuum* **2021**, *193*, 110545.
25. De Souza Lamim, T.; Bernardelli, E.; Bendo, T.; Melo, C.H.; Binder, C.; Klein, A. Duplex surface treatment of sintered iron by plasma nitriding and plasma carburizing at low temperature. *Surf. Coat. Technol.* **2019**, *375*, 911–919. [CrossRef]
26. Moskalioviene, T.; Galdikas, A. Mechanisms of the Hydrogen Influence on the Diffusivity of Nitrogen During Plasma Nitriding Austenitic Stainless Steel. *Metall. Mater. Trans. A* **2019**, *50*, 1021–1032. [CrossRef]
27. Dalke, A.; Burlacov, I.; Hamann, S.; Puth, A.; Böcker, J.; Spies, H.J.; Röpcke, J.; Biermann, H. Solid carbon active screen plasma nitrocarburizing of AISI 316L stainless steel: Influence of N_2-H_2 gas composition on structure and properties of expanded austenite. *Surf. Coat. Technol.* **2019**, *357*, 1060–1068. [CrossRef]
28. Vasyliev, G.; Pylypenko, I.; Kuzmenko, O.; Gerasymenko, Y. Fouling influence on pitting corrosion of stainless steel heat exchanging surface. *Therm. Sci. Eng. Prog.* **2022**, *30*, 101278. [CrossRef]
29. Messinese, E.; Casanova, L.; Paterlini, L.; Capelli, F.; Bolzoni, F.M.; Ormellese, M.; Brenna, A. A Comprehensive Investigation on the Effects of Surface Finishing on the Resistance of Stainless Steel to Localized Corrosion. *Metals* **2022**, *12*, 1751. [CrossRef]
30. Gokcekaya, O.; Ergun, C.; Gulmez, T.; Nakano, T.; Yilmaz, S. Structural Characterization of Ion Nitrided 316L Austenitic Stainless Steel: Influence of Treatment Temperature and Time. *Metals* **2022**, *12*, 306.
31. Dib, J.; Gómez, B.; Strubbia, R.; Ares, A.; Méndez, C.; Fuster, V.; Hereñu, S. Characterization of Plasma Nitrided Duplex Stainless Steel: Influence of Prior Shot Peening and Nitriding Atmosphere. *J. Mater. Eng. Perform.* **2023**, *32*, 406–414. [CrossRef]
32. Frączek, T.; Prusak, R.; Ogórek, M.; Skuza, Z. Nitriding of 316L Steel in a Glow Discharge Plasma. *Materials* **2022**, *15*, 3081. [CrossRef] [PubMed]
33. Lynch, B.; Wang, Z.; Ma, L.; Paschalidou, E.M.; Wiame, F.; Maurice, V.; Marcus, P. Passivation-Induced Cr and Mo Enrichments of 316L Stainless Steel Surfaces and Effects of Controlled Pre-Oxidation. *J. Electrochem. Soc.* **2020**, *167*, 141509. [CrossRef]
34. Mroczkowska, K.; Dzienny, P.; Budnicki, A.; Antonczak, A. Corrosion Resistance of AISI 304 Stainless Steel Modified Both Femto- and Nanosecond Lasers. *Coatings* **2021**, *11*, 592. [CrossRef]
35. Ruiz, A.; Hernández, H.; Hernández, J.; Orozco-Cruz, R.; Ruiz-Reynoso, A.; González, C.; Miranda-Hernández, J. Electrochemical Impedance Spectroscopy (EIS): A Review Study of Basic Aspects of the Corrosion Mechanism Applied to Steels. *Electrochem. Impedance Spectrosc.* **2020**, 94470. [CrossRef]

Disclaimer/Publisher's Note: The statements, opinions and data contained in all publications are solely those of the individual author(s) and contributor(s) and not of MDPI and/or the editor(s). MDPI and/or the editor(s) disclaim responsibility for any injury to people or property resulting from any ideas, methods, instructions or products referred to in the content.